Bond Graph Modeling of Mechanical Circulatory Support Device—Cardiovascular System Interactions

Mengtang Li
Department of Mechanical Engineering,
Vanderbilt University,
2301 Vanderbilt Place,
Nashville, TN 37235
e-mail: mengtang.li@vanderbilt.edu

Marvin J. Slepian
Department of Biomedical Engineering,
Sarver Heart Center University of Arizona,
1501 N Campbell Avenue,
Tucson, AZ 85724;
Department of Medicine,
Sarver Heart Center University of Arizona,
1501 N Campbell Avenue,
Tucson, AZ 85724
e-mail: chairman.syns@gmail.com

Eric J. Barth
Department of Mechanical Engineering,
Vanderbilt University,
2301 Vanderbilt Place,
Nashville, TN 37235
e-mail: eric.j.barth@vanderbilt.edu

Though mechanical circulatory support (MCS) devices, such as ventricular assist devices and total artificial hearts (TAH), provide heart failure patients with bridges to heart transplantation or are alternatives to transplantation, device performance, and corresponding control strategies are often difficult to evaluate. Difficulties arise due to the complex interaction of multiple domains—i.e., biological, hydraulic, hemodynamics, electromechanical, system dynamics, and controls. In an attempt to organize, integrate and clarify these interactions, a technique often used in hydraulic pump design and robotics, called "bond graph modeling," is applied to describe the performance and functionality of MCS devices and the interaction between the cardiovascular (CV) system and the MCS device. This technical brief demonstrates the advantages of this tool in formulating a model for the systemic circulation interacting with the left side of a TAH, adopting the fundamental structure of either a hydraulic mechanism (i.e., AbioCor/Carmat) or a pneumatic mechanism (i.e., SynCardia), combined with a systemic circulation loop. The model captures the dynamics of the membrane, the hydraulic source or pneumatic source, and the systemic circulation. This multidisciplinary cross-pollination of an analytical tool from the field of dynamic systems may provide important insight to further aid and improve the design and control of future MCS systems.
[DOI: 10.1115/1.4045812]

1 Introduction

A "bond graph" is a graphical modeling method to describe the energy relationship within any physical dynamic system [1,2]. Although seemingly similar to a block diagram or a signal flow graph, a bond graph mainly represents bidirectional energy exchange flows, instead of unidirectional information flows. Energy ports are linked via bonds. The energy flow within each bond is denoted by a pair of power variables called "effort" and "flow," whose product is the instantaneous power flowing through that bond (e.g., force × velocity, pressure × flowrate, voltage × current). Energy ports are connected together with 0-junctions, where the effort over all connected bonds is the same while the flows sum to zero, and 1-junctions, where the flow through all connected bonds is the same while the efforts sum to zero. A unified model can be derived for multi-energy-domain systems using this method. Another significant feature of a bond graph is the causality, which indicates the feasibility of mathematical relationships in the real world. One dominant power variable (e.g., voltage) eventually specifies the other one (e.g., current), with the whole system energy exchange mechanism known (e.g., impedance). The effort and flow variables form a "handshake" mechanism between dynamic elements. In this manner, bond graphs allow modeling of subsystems with a first-principles mechanism of interaction with connected subsystems. Even though the cardiovascular system and mechanical circulatory support device are very different, the bond graph methodology allows us to study their multi-energy-domain interaction.

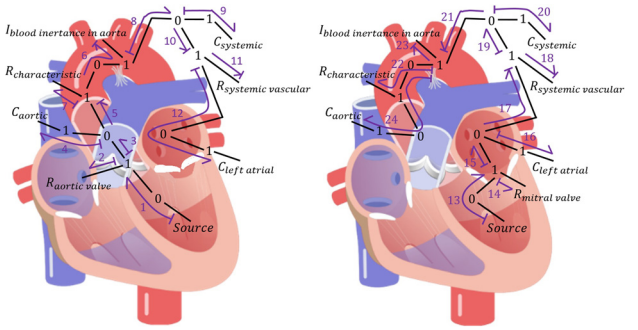

(*a*) (*b*)

Fig. 1 (*a*) Bond graph graphic modeling of ejection phase. (*b*) Bond graph graphic modeling of injection phase.

2 Modeling

Research has been done to develop accurate models for the human circulation, including systemic and pulmonary circulations [3–7] and on the interdependence between the two sides [8]. Using a bond graph representation, such models can be paired with models of MCS devices to study their interactions [9,10]. To illustrate the bond graph technique, using a model similar to the cardiovascular system as described in Ref. [7], the interaction of the systemic circulation with one side of a total artificial hearts system is considered here. Distinct pressure locations are marked with 0-junctions and connected with cardiovascular elements through 1-junctions, as shown in Figs. 1(a) and 1(b). The bond graph energy bonds (purple line with half arrow and end bar) were then obtained and marked by numbers. Due to four different modes of these two valves, three different cardiac phases, i.e., ejection phase, injection phase and isovolumetric phase, exist. Considering that only passive valves are used in currently available TAHs (Syncardia), such as the U.S. Food and Drug Administration (FDA) approved rotating disk valve [11], the isovolumetric phase is not modeled here for the systemic circulation combined with a TAH.

2.1 Ejection Phase Modeling. During the ejection phase, the aortic valve is open while the mitral valve is closed. The bond graph equations Eqs. (1)–(17) are derived below. The left atrial pressure (LAP), arterial pressure (AP), aortic pressure (AoP),

Manuscript received June 3, 2019; final manuscript received November 25, 2019; published online March 4, 2020. Assoc. Editor: Alison Marsden.

aortic flowrate, and outlet flowrate from the TAH are e_{12}, e_9, e_4, f_6, and f_1, respectively.

$$f_1 = f_2 = f_3 \tag{1}$$
$$e_1 = e_2 + e_3 \tag{2}$$
$$e_2 = R_3 f_2 \tag{3}$$
$$e_3 = e_4 = e_5 \tag{4}$$
$$f_3 = f_4 + f_5 \tag{5}$$
$$\dot{e}_4 = (1/C_4) f_4 \tag{6}$$
$$f_5 = f_6 = f_7 = f_8 \tag{7}$$
$$e_5 = e_6 + e_7 + e_8 \tag{8}$$
$$\dot{f}_6 = (1/I) e_6 \tag{9}$$
$$e_7 = R_4 f_7 \tag{10}$$
$$e_8 = e_9 = e_{10} \tag{11}$$
$$f_8 = f_9 + f_{10} \tag{12}$$
$$\dot{e}_9 = (1/C_3) f_9 \tag{13}$$
$$f_{10} = f_{11} = f_{12} \tag{14}$$
$$e_{10} = e_{11} + e_{12} \tag{15}$$
$$e_{11} = R_1 f_{11} \tag{16}$$
$$\dot{e}_{12} = (1/C_2) f_{12} \tag{17}$$

2.2 Injection Phase Modeling. During the injection phase, the aortic valve is closed while the mitral valve is open. The bond graph model equations Eqs. (18)–(34) are derived below. The LAP, AP, AoP, aortic flowrate, and inlet flowrate from TAH are e_{16}, e_{20}, e_{24}, f_{23}, and f_{13}, respectively.

$$f_{13} = f_{14} = f_{15} \tag{18}$$
$$e_{13} = e_{14} + e_{15} \tag{19}$$
$$e_{14} = R_2 f_{14} \tag{20}$$
$$e_{15} = e_{16} = e_{17} \tag{21}$$
$$f_{15} = f_{16} + f_{17} \tag{22}$$
$$\dot{e}_{16} = (1/C_2) f_{16} \tag{23}$$
$$f_{17} = f_{18} = f_{19} \tag{24}$$
$$e_{17} = e_{18} + e_{19} \tag{25}$$
$$e_{18} = R_1 f_{18} \tag{26}$$
$$e_{19} = e_{20} = e_{21} \tag{27}$$
$$f_{19} = f_{20} + f_{21} \tag{28}$$
$$\dot{e}_{20} = (1/C_3) f_{20} \tag{29}$$
$$f_{21} = f_{22} = f_{23} = f_{24} \tag{30}$$
$$e_{21} = e_{22} + e_{23} + e_{24} \tag{31}$$
$$e_{22} = R_4 f_{22} \tag{32}$$
$$\dot{f}_{23} = (1/I) e_{23} \tag{33}$$
$$\dot{e}_{24} = (1/C_4) f_{24} \tag{34}$$

2.3 Hydraulic-Based Total Artificial Hearts Modeling. A self-contained implantable MCS device, the Carmat TAH, consists of two independent ventricles separated by membranes into compartments for blood and hydraulic oil, four tricuspid valves for unidirection flow, internal battery and transcutaneous energy

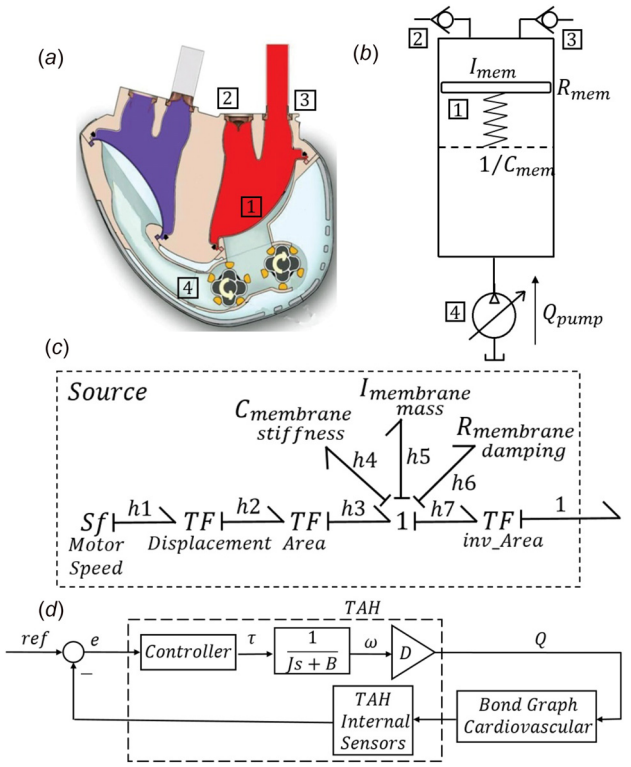

Fig. 2 (*a*) Cross-sectional view of Carmat TAH: ① membrane, ② inlet valve, ③ outlet valve, ④ gear pumps. (*b*) Simplified dynamic model of Carmat TAH. (*c*) Bond graph of Carmat TAH. (*d*) Control block diagram.

transfer coils, as shown in Fig. 2(*a*). Two external gear pumps are placed below the two ventricles and rotate back and forth to pump hydraulic oil to move the membranes, thus creating a pulsatile blood flow [12]. The fundamental pumping mechanism of the Carmat TAH can be modeled as a mass-spring-damper system powered by a controllable flow source, as in Fig. 2(*b*). The elastic membrane is considered as a solid piston while its elasticity is modeled by spring stiffness and damping. The simplified bond graph model is shown in Fig. 2(*c*) and corresponding Eqs. (35)–(46) are derived as follows:

$$f_{h1} = S_f \tag{35}$$
$$f_{h2} = D f_{h1} \tag{36}$$
$$e_{h1} = D e_{h2} \tag{37}$$
$$f_{h3} = (1/A_{\text{mem}}) f_{h2} \tag{38}$$
$$e_{h2} = (1/A_{\text{mem}}) e_{h3} \tag{39}$$
$$f_{h3} = f_{h4} = f_{h5} = f_{h6} = f_{h7} \tag{40}$$
$$e_{h3} = e_{h4} + e_{h5} + e_{h6} + e_{h7} \tag{41}$$
$$\dot{e}_{h4} = (1/C_{\text{mem}}) f_{h4} \tag{42}$$
$$\dot{f}_{h5} = (1/I_{\text{mem}}) e_{h5} \tag{43}$$
$$e_{h6} = R_{\text{mem}} f_{h6} \tag{44}$$
$$f_1 = A_{\text{mem}} f_{h7} \tag{45}$$
$$e_{h7} = A_{\text{mem}} e_1 \tag{46}$$

With 16 unknowns but only 15 equations, the following restriction or relation can be obtained

$$f_1 = D S_f \tag{47}$$

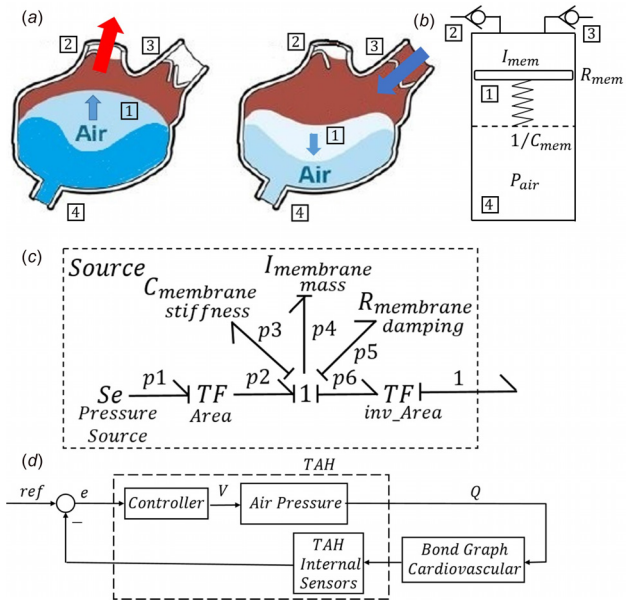

Fig. 3 (*a*) Cross view of SynCardia TAH: ① membrane, ② outlet valve, ③ inlet valve, ④ external pressure source. (*b*) Simplified dynamic model of SynCardia TAH. (*c*) Bond graph model of SynCardia TAH. (*d*) Control block diagram.

which means the flowrate of the hydraulic pump determines the flowrate of the TAH directly without the effect of the cardiovascular system. Once the driving signal, pump speed $S_f = f_{h1}$, is given, the equation set is solvable and the interaction between the TAH and the circulation system can be simulated and analyzed.

2.4 Pneumatic-Based Total Artificial Hearts Modeling. As the only FDA approved TAH for use as a bridge to transplantation (2004) and for long-term (destination) implantation (2012), the SynCardia heart, shown in Fig. 3(*a*), is composed of two independent polyurethane ventricles with 70 mL volume, four mechanical valves for unidirectional flow control, and two percutaneous pneumatic tubes for connecting to the external console. Blood inflow and ejection motion is realized by the membranes which are controlled by a pneumatic pressure differential across the membranes. The dynamic mechanism of the membrane can be modeled as a mass-spring-damper system powered by a controllable pressure source, as in Fig. 3(*b*). The semi-elastic membrane is considered as a solid piston while its elasticity is modeled by spring stiffness and damping. The simplified bond graph model is shown in Fig. 3(*c*). As mathematically proven in Eq. (47) previously, the TAH flowrate equals that of the source. While for the hydraulic-based TAH, such as the Carmat or AbioCor, the source flow is known (specified by the controlled motor speed), for the pneumatic-based TAH, such as SynCardia, the flow from the source is unknown and it depends on the interaction with the rest of the cardiovascular system (pressure is the specified effort source).

The dynamic model of the pneumatic power mass-spring-damper system is described as follows:

$$f_1 = f_{p1} \tag{48}$$

$$I_{\text{mem}}\ddot{f}_{p2} = A_{\text{mem}}(e_{p1} - e_1) - R_{\text{mem}}\dot{f}_{p2} - C_{\text{mem}}f_{p2} \tag{49}$$

$$f_1 = A_{\text{mem}}f_{p2} \tag{50}$$

$$e_1 = \begin{cases} \text{AoP} + R_3 f_1, & \text{if } f_1 > 0 \\ \text{LAP} + R_2 f_1, & \text{if } f_1 < 0 \end{cases} \tag{51}$$

Once the driving signal, air pressure $S_e = e_{p1}$, is given, the equation set is solvable and the interaction between the TAH and the circulation system can be simulated and analyzed.

3 Results

Various methods and tools exist to solve the bond graph model. Our results demonstrate that the model can be utilized to investigate the effects of either varying cardiovascular (CV) conditions

Table 1 Bond graph model parameters

Symbol	Description	Value
Systemic circulation		
R_1	Systemic vascular resistance	0.6667–2.6667 × 10^{-4} (kPa s /mm^3)
R_2	TAH inlet valve resistance	6.6661 × 10^{-7} (kPa s/mm^3)
R_3	TAH outlet valve resistance	1.3332 × 10^{-7} (kPa s/mm^3)
R_4	Characteristic resistance	5.3062 × 10^{-6} (kPa s/mm^3)
C_2	Left atrial compliance	3.3003 × 10^4 (mm^3/kPa)
C_3	Systemic compliance	9.9758 × 10^3 (mm^3/kPa)
C_4	Aortic compliance	6.0005 × 10^2 (mm^3/kPa)
I	Inertance of blood in aorta	6.6661 × 10^{-8} (kPa s^2/mm^3)
$E_{\max}$	ESPVR constant	2.6 × 10^{-4} (mm^3)
$E_{\min}$	EDPVR constant	0.08 × 10^{-4} (mm^3)
V_0	Reference volume at 0 pressure	10 × 10^3 (mm^3)
HR	Heart beat frequency	75 (bpm)
Hydraulic-based TAH		
A_{mem}	Effective surface area of membrane	2.83 × 10^{-3} (m^2)
C_{mem}	Reciprocal of membrane spring stiffness	10^{-2} to 10^{-1} (mm/mN)
I_{mem}	Membrane mass	5 × 10^{-2} (kg)
R_{mem}	Membrane damping	1–10 (mN s/mm)
B	Rotary damping of motor+pump	50–500 × 10^{-7} (kg m^2/s)
D	Gear pump displacement	50 × 10^3 (mm^3)
J	Moment of inertia of motor+pump	50–200 × 10^{-7} (kg m^2)
Pneumatic-based TAH		
A_{mem}	Effective surface area of membrane	2.83 × 10^{-3} (m^2)
I_{mem}	Membrane mass	5 × 10^{-2} (kg)
C_{mem}	Reciprocal of membrane spring stiffness	10^{-2}–10^{-1} (mm/mN)
R_{mem}	Membrane damping	1–10 (mN s/mm)
$V_{\max}$	Total chamber volume	70 × 10^3 (mm^3)

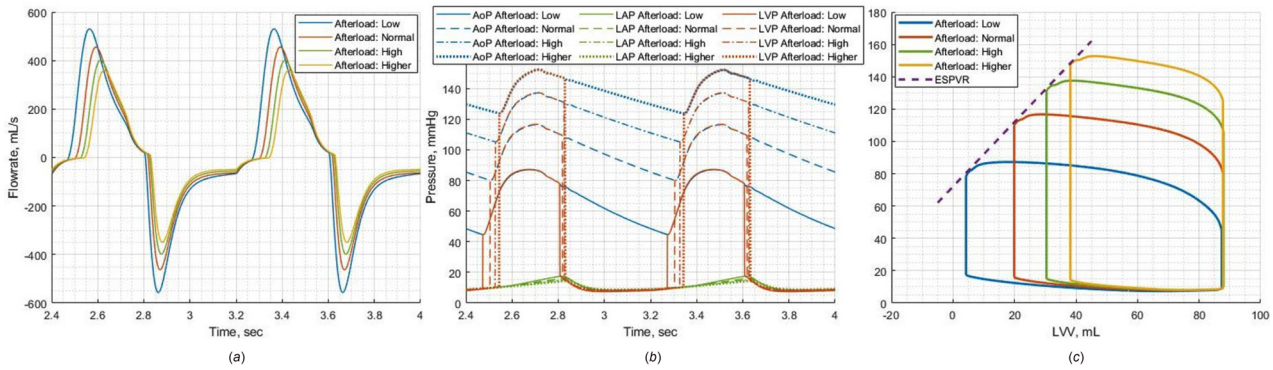

Fig. 4 (*a*) Flowrate versus time. (*b*) Pressure versus time. (*c*) Pressure-volume (PV)-loops of the hydraulic-based TAH with different afterload.

Table 2 Hemodynamic parameters for the hydraulic-based TAH with different afterload

Afterload (mmHg s/mL)	Stroke volume (mL)	Cardiac output (LPM)	AoP (mmHg) sys/dia/mean	LAP (mmHg) max/min/mean
0.5	83.82	6.2867	87.07/44.58/67.21	17.63/7.99/11.08
1.0	68.19	5.1143	116.52/77.99/99.35	16.19/8.32/10.98
1.5	57.59	4.3193	137.24/105.16/121.92	15.31/8.54/10.88
2.0	50.01	3.7508	152.33/123.62/138.41	14.58/8.65/10.72

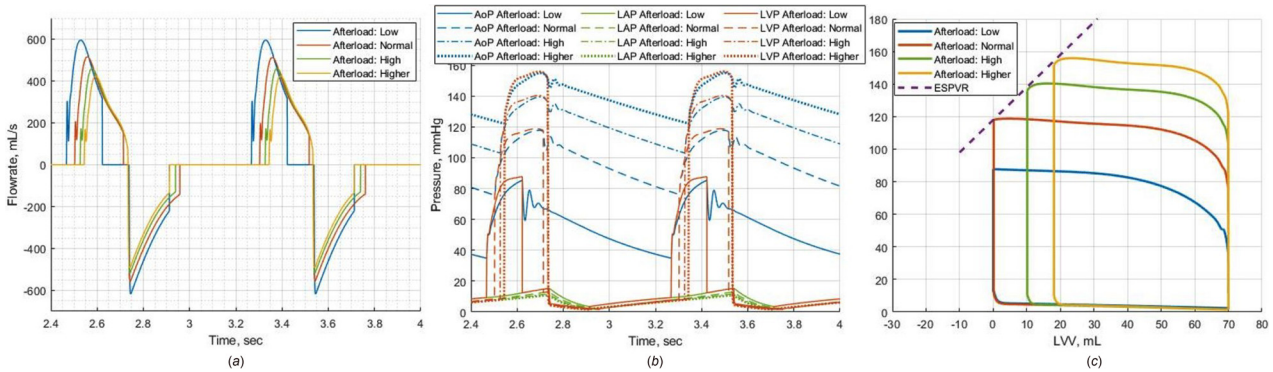

Fig. 5 (*a*) Flowrate versus time. (*b*) Pressure versus time. (*c*) PV-loops of the pneumatic-based TAH with different afterload.

Table 3 Hemodynamic parameters for the pneumatic-based TAH with different afterload

Afterload (mmHg s/mL)	Stroke volume (mL)	Cardiac output (LPM)	AoP (mmHg) sys/dia/mean	LAP (mmHg) max/min/mean
0.5	70	5.2500	85.31/34.87/56.07	15.36/3.51/8.84
1.0	70	5.2500	117.86/75.72/97.41	13.15/2.07/7.02
1.5	59.94	4.4955	139.40/103.03/121.78	11.75/1.91/6.42
2.0	52.03	3.9022	155.06/122.18/138.72	10.92/1.95/6.18

encoded by the model's parameters (e.g., afterload) or altering mechanical properties of the TAH (e.g., damping, moment of inertia of the pump rotor, or stiffness of the pneumatic membrane). Such investigation is useful in evaluating a particular design and thereby guide and improve any model-guided design iteration. The hydraulic and pneumatic based TAHs are controlled to track a cardiac output and flowrate emulating a human heart [13], with the associated control block diagram shown in Figs. 2(*d*) and 3(*d*), respectively.

Bond graph model parameters for the systemic circulation [14] and hydraulic and pneumatic-based TAHs are listed in Table 1. To ensure the correctness and consistency of the modeling from the energy point of view, SI units are used and then converted into medical standard units. All simulations were run under steady-state body conditions and control algorithms and gains for TAHs to run in response to varying conditions were kept the same since the specific control design is out of scope of this technical brief.

3.1 Hydraulic-Based Total Artificial Hearts + Circulation. + Circulation. The hemodynamics of the hydraulic-based TAH circulation system under four different afterload operating conditions are shown in Fig. 4 (Table 2). As the afterload increases, higher LVP is required to open aortic valve to eject blood into aorta. The delayed valve open time and decreased blood pumping effects are also noticeable from Figs. 4(*a*) and 4(*b*). Note that

compared with the native heart, the blood pumping chamber of this hydraulic based TAH is smaller (to fit the entire device in a patient's chest), which leads the end systolic pressure volume relationship (ESPVR) in Fig. 4(*c*) intersects with horizontal axis at a different location.

3.2 Pneumatic-Based Total Artificial Hearts + Circulation. + Circulation. Unlike the hydraulic-based TAH, the control strategy for a pneumatic-based TAH is more complex as is shown by Eq. (62) and Eqs. (63)–(66). Figure 5 plots the hemodynamics of the pneumatic-based TAH circulation system under four different afterload operating conditions (Table 3). Reduced pressure required to open aortic valve, delayed valve opening time, and decreased amount of pumping blood due to increased afterload pressure can be seen from Fig. 5. Also, compared with the native heart, the blood pumping chamber of a pneumatic-based TAH (e.g., 70 mL for SynCardia) is smaller in size to fit within the patient's chest. The consequence of this smaller size, at least for this control algorithm, is that it cannot comply with the ESPVR once it reaches the volume limits, as the blue PV-loop shown in Fig. 5(*c*).

4 Conclusions

The net performance of implanted MCS devices involves the balance of interaction between the device and the overall cardiovascular system of the individual patient into whom it is implanted. Bond graph modeling provides a quantitative methodology for universally describing a complex system containing subsystems from the perspective of differing energy domains. This technical brief highlights this methodology to suggest its value, and offer it as a tool to further understand MCS–human CV system interactions, as well as to examine the behavior of parameters and variables which may be optimized to enhance device and system design. This approach adds an additional tool to the cardiovascular biomechanical engineer, physiologist, and physician with potential for enhancing the safety and efficacy of MCS systems, thereby reducing adverse events and improving their clinical utility.

5 Limitations

Here, we present only a simple bond graph model describing the interaction between the systemic circulation loop with the left side of a basic TAH. A more detailed model is needed to take into account the right (pulmonary) side of the heart and interdependence between left and right sides, isovolumetric phase, and the dynamics of heart valves. What we present is a starting point, as ultimately further model validation will be needed. Finally, we must keep in mind that the traditional bond graph technique utilizes SI units during calculation, resulting in uncommon medical standard units.

Acknowledgment

We acknowledge support for the Arizona Center for Accelerated Biomedical Innovation (ACABI) of the University of Arizona.

References

[1] Paynter, H. M., 1961, *Analysis and Design of Engineering Systems*, MIT Press, Cambridge, MA.

[2] Karnopp, D., and Rosenberg, R. C., 1968, "Analysis and Simulation of Multiport Systems: The Bond Graph Approach to Physical System Dynamics," MIT Press, Cambridge, MA.

[3] Bai, J., Ying, K., and Jaron, D., 1992, "Cardiovascular Responses to External Counterpulsation: A Computer Simulation," Med. Biol. Eng. Comput., **30**(3), pp. 317–323.

[4] De Lazzari, C., Ferrari, G., Mimmo, R., Tosti, G., and Ambrosi, D., 1994, "A Desk-Top Computer Model of the Circulatory System for Heart Assistance Simulation: Effect of an LVAD on Energetic Relationships Inside the Left Ventricle," Med. Eng. Phys., **16**(2), pp. 97–103.

[5] Xu, L., and Fu, M., 2000, "Computer Modeling of Interactions of an Electric Motor, Circulatory System, and Rotary Blood Pump," ASAIO J., **46**(5), pp. 604–611.

[6] Ferreira, A., Chen, S., Simaan, M. A., Boston, J., and Antaki, J. F., 2005, "A Nonlinear State-Space Model of a Combined Cardiovascular System and a Rotary Pump," Proceedings of the 44th IEEE Conference on Decision and Control, Seville, Spain, Dec. 12–15, IEEE, pp. 897–902.

[7] Simaan, M. A., Ferreira, A., Chen, S., Antaki, J. F., and Galati, D. G., 2009, "A Dynamical State Space Representation and Performance Analysis of a Feedbackcontrolled Rotary Left Ventricular Assist Device," IEEE Trans. Control Syst. Technol., **17**(1), pp. 15–28.

[8] Santamore, W. P., and Burkhoff, D., 1991, "Hemodynamic Consequences of Ventricular Interaction as Assessed by Model Analysis," Am. J. Physiol.: Heart Circ. Physiol., **260**(1), pp. H146–H157.

[9] Klute, G., Tasch, U., and Geselowitz, D., 1992, "An Optimal Controller for an Electric Ventricular-Assist Device: Theory, Implementation, and Testing," IEEE Trans. Biomed. Eng., **39**(4), pp. 394–403.

[10] Tsach, U., Geselowitz, D., Sinha, A., and Hsu, H., 1989, "A Novel Output Feedback Pusher Plate Controller for the Penn State Electric Ventricular Assist Device," ASME J. Dyn. Syst. Meas. Control, **111**(1), pp. 69–74.

[11] Slepian, M. J., Alemu, Y., Soares, J. S., Smith, R. G., Einav, S., and Bluestein, D., 2013, "The syncardia™ Total Artificial Heart: In Vivo, In Vitro, and Computational Modeling Studies," J. Biomech., **46**(2), pp. 266–275.

[12] Mohacsi, P., and Leprince, P., 2014, "The Carmat Total Artificial Heart," Eur. J. Cardiothorac. Surg., **46**(6), pp. 933–934.

[13] Lankhaar, J.-W., RÖvekamp, F. A., Steendijk, P., Faes, T. J., Westerhof, B. E., Kind, T., Vonk-Noordegraaf, A., and Westerhof, N., 2009, "Modeling the Instantaneous Pressure–Volume Relation of the Left Ventricle: A Comparison of Six Models," Ann. Biomed. Eng., **37**(9), pp. 1710–1726.

[14] Yu, Y.-C., Boston, J. R., Simaan, M. A., and Antaki, J. F., 1998, "Estimation of Systemic Vascular Bed Parameters for Artificial Heart Control," IEEE Trans. Autom. Control, **43**(6), pp. 765–778.